Journal of
Materials Chemistry A

Accepted Manuscript

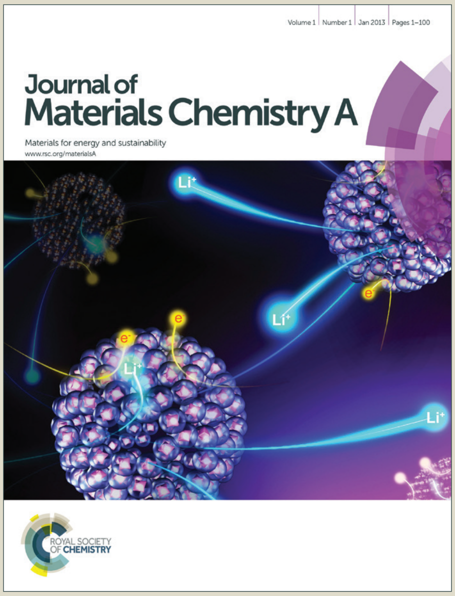

Volume 1 | Number 1 | Jan 2013 | Pages 1–100

Journal of Materials Chemistry A

Materials for energy and sustainability

www.rsc.org/materialsA

ROYAL SOCIETY
OF CHEMISTRY

www.rsc.org/materialsA

Encapsulating sulfur into hybrid porous carbon/CNTs substrate as cathode for lithium-sulfur batteries

Ze Zhang, Hang-Kun Jing, Sheng Liu, Guo-Ran Li and Xue-Ping Gao*

TOC

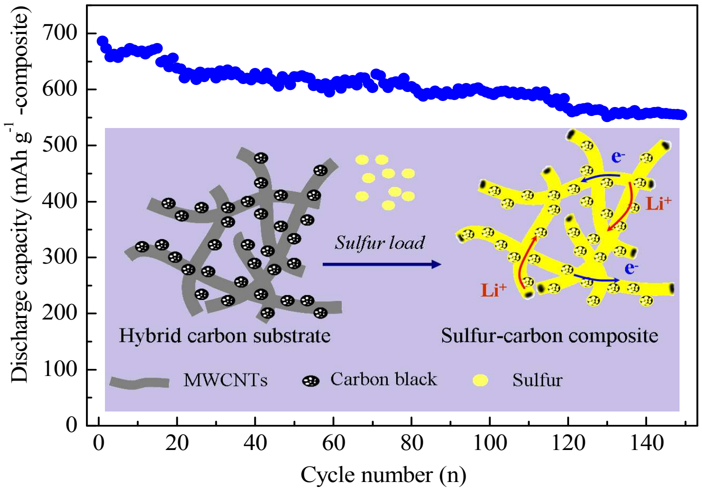

A facile sulfur/carbon multi-composite with high sulfur content, consisting of sulfur and the commercial carbon materials (CNTs and carbon black), exhibits excellent cycle performance for lithium-sulfur batteries.

Journal of
Materials Chemistry A

Cite this: DOI: 10.1039/c0xx00000x

www.rsc.org/xxxxxx

ARTICLE TYPE

Encapsulating sulfur into hybrid porous carbon/CNTs substrate as cathode for lithium-sulfur batteries

Ze Zhang, Hang-Kun Jing, Sheng Liu, Guo-Ran Li and Xue-Ping Gao*

Received (in XXX, XXX) Xth XXXXXXXXX 20XX, Accepted Xth XXXXXXXXX 20XX
DOI: 10.1039/b000000x

Hybrid carbon substrate as sulfur immobilizer is obtained via simple processes to fabricate cathode material for lithium-sulfur batteries. The microstructure and morphology of the sulfur/carbon composites are characterized by X-ray diffraction (XRD), scanning electron microscopy (SEM) and transmission electron microscopy (TEM). It is demonstrated that commercial carbon black and multi-walled carbon nanotubes (CNTs) are cooperated with each other well with an appropriate mass ratio in the hybrid substrate. In particular, the large sulfur content of 81.7 wt% can be loaded into to the hybrid carbon substrate forming the sulfur/carbon composite. When the mass ratio of carbon black and CNTs is 1 : 1, the composite delivers a high initial capacity of 837.3 and 685.9 mA h g^{-1}(composite) at the current densities of 80 and 160 mA g^{-1}(composite) based on the composite as cathode-active material. The discharge capacity remains at 554.4 mA h g^{-1}(composite) at the current density of 160 mA g^{-1}(composite) after 150 cycles, indicating a low capacity fading of about 0.12 % per cycle. Besides, the composite offers high Coulombic efficiency about 100 %. The significant improvements in electrochemical performance are associated with the desirable combination of carbon black and CNTs in the hybrid carbon substrate. Therefore, this work proposes a low-cost and effortless approach to prepare sulfur/carbon composites with high performance as cathode for lithium-sulfur batteries.

Introduction

With the ever-increasing thirst for high energy storage systems by the society, it is imperative to explore high-energy-density and long cycling stability rechargeable batteries.[1,2] Among the multitudinous cathode materials, element sulfur is a promising candidate because of its two-electron reaction with Li yielding a high theoretical specific capacity of 1675 mA h g^{-1} for sulfur, leading to a high theoretical energy density of 2600 W h kg^{-1} for lithium-sulfur (Li-S) batteries.[3–6] Besides, sulfur shows some other outstanding features, such as high nature abundance, low cost and nontoxic.[7] Nonetheless, Li-S batteries have been plagued by a series of problems, including intrinsically non-conducting sulfur and its final lithiated product (Li_2S), the dissolution and diffusion of intermediate lithium polysulfide, and large volume expansion of sulfur upon lithiation, resulting in the poor cycle stability.[6,8–13]

Recently, tremendous efforts had been put into improving the electrochemical performance of Li-S batteries, including the optimization of electrolyte system,[14–21] the use of various carbon materials,[3,22–42] and the coating of conducting polymers.[43–48] As a crucial component of sulfur cathodes, carbon materials have been demonstrated to be practicable in handling the aforementioned problems because of their abundant pore structures and high electronic conductivity. Among the various carbon materials, micro-/mesoporous carbon, can be used as the host of sulfur for Li-S batteries, which can possess high electronic conductivity and trap well polysulfide species, therefore increasing the utilization of active sulfur and suppressing polysulfide shuttling at low rates.[22–26] It is notable that the pore structure of carbon material can be easily adjusted by KOH, thus increasing the sulfur content in sulfur/carbon (S/C) composite.[27] In comparison, carbon nanotube (CNT), as a typical 1D carbon material, can be assembled into a conducting network, where nanotubes are interpenetrated with each other, and used as substrate for fixing sulfur.[33–41] More importantly, the large aspect ratio with sufficient surface makes CNTs to affix sulfur, as well as efficient pathway for electron, thus enhancing the rate capability of sulfur cathode.[33,38,41] However, the low sulfur content in S/CNTs composites remain intractable issues. It is important but also difficult to increase the sulfur content in the composite while retaining its high sulfur utilization simultaneously. In addition, with the mass production and commercialization of both carbon black and CNTs, the fabrication of S/C composites for Li-S batteries is one of the more promising options. Therefore, the key is how to take full use of the respective advantages of different carbon materials to enhance the electrochemical performance of S/C composites.

Based on the aforementioned consideration, fabricating the multi-composites of sulfur and carbon materials, in which different carbon materials can well cooperate with each other to enhance the electrochemical performance of the cathode, should be a practicable and considerable strategy to promote the idea. For example, CNTs-core/porous-carbon-shell structure,[49,50] and three-dimensional (3D) graphene-based structure,[51–55] are designed to stable sulfur accommodation, and the Li-S batteries based on such multi-composites afford enhanced super-capacitive performance owing to the synergistic effect of the different carbon components.

Meanwhile, it should be notable that a large sulfur content (at least over 70 wt %) in the S/C composites is really indispensable for high capacity of sulfur cathode and high practical energy density of Li-S batteries.[11–12] However, only a limited quantity of the desirable carbon materials can be synthesized and the process involves various hard or soft templates and the carbonization at high temperature. As to synthesize the graphene-based hybrid carbon substrate, it is relatively complex and also involves some strong oxidants and concentrated acid. For the sake of saving energy and reducing the cost, seeking the stable, abundant, and applicable carbon materials with desirable pore structure is essential for effortless methods to prepare S/C composites.

Here, our concept involves adopting commercial carbon black and multi-walled CNTs to easily prepare a hybrid carbon substrate to fabricate the S/C composite as cathode for Li-S batteries. It should attract more attention here that the use of the commercial and low-cost carbon black and CNTs as carbon substrates and the relatively simple synthetic process. In the designed hybrid substrate, carbon black, trapping sulfur in its abundant pores, is either forced into the inner diameter of CNTs, or attached to the outer wall of CNTs after the treatments. Moreover, multi-walled CNTs are intertwined with one other to form a web-like structure for the transfer of both electrons and Li ions. With the synergistic combination of this two carbon components, the as-prepared S/C composite presents a desirable improvement of the electrochemical performance as cathode for Li-S battery.

Experimental section

Preparation of S/A-MCxy composites

The carbon black (“C”, PBX-51, Cabot Corporation) was firstly mixed with multi-walled CNTs (“M”, L-CNTs-2040, Shenzhen Nanotech Port Co. Ltd) at the mass ratio of 1 : 1, and ball-milled at the speed of 250 rpm for 12 h. Then the mixture was activated with KOH, marked as A-MC11. The exact process of activation can be referred to elsewhere.[27] The S/A-MC11 composite was prepared via a typical melt-diffusion method. The A-MC11 carbon substrate was thoroughly ground with sulfur powder (Alfa Aesar, >99.5%) in a sealed vessel, and heated for 12 h at 155 ℃, followed by another 2 h at 300 ℃ under an argon atmosphere to fabricate the S/C composite with a sulfur content of about 80 wt %. As comparison, another two samples with different mass ratios of the two carbon components were synthesized in the same way, marked as S/A-MC12 and S/A-MC21 respectively. Here, the numbers in the marks stand for the mass ratio of the two carbon components. In general, A-MCxy means CNTs : carbon black = x : y (w/w).

Structural characterization

The structure of the as-prepared S/C composites was measured by X-ray diffraction (XRD, Rigaku mini Flex Ⅱ) with 2θ range from 10 to 80°. The sulfur content in the S/C composites was confirmed by using a thermogravimetric analyzer (METTLER TOLEDO, TGA/DSC1) under argon atmosphere with a heating rate of 10 ℃ min^{-1} from 50 to 800 ℃. The microstructure and morphology of the composites were identified by Fourier transform infrared (FTIR, Tensor 27, Bruker), scanning electron microscopy (SEM, Supra 55VP) and transmission electron microscopy (TEM, FEI, Tecnai F20).

Electrochemical measurement

In order to prepare the working electrode, the as-prepared S/C composites were firstly mixed with Super P and PVDF at the mass ratio of 70 : 20 : 10, and dispersed in N-methyl-2-pyrrolidone (NMP) solvent to form a slurry. Then, the slurry was coated onto an aluminum foil current collector and dried in vacuum oven at 50 ℃ for 12 h. Finally, the film on the aluminum foil was punched into a film disk with a diameter of 12 mm with the sulfur loading of 1.2–1.5 mg cm^{-2}. 2032-type coin cells were assembled in a glove box filled with argon. Lithium foil was used as the counter and reference electrode, and Celgard 2300 was used as a separator. The electrolyte was consisted of 1.0 M LiTFSI in 1,3-dioxolane (DOL) and 1,2-dimethoxyethane (DME) (v/v 1 : 1) with 0.2 M $LiNO_3$ as an additive. Charge and discharge tests of the cells were carried out at the current density of 160 mA g^{-1} between 1.7 and 2.8 V (*vs.* Li/Li^+) at room temperature using a LAND-CT2001A instrument (Wuhan Jinnuo, China). The specific capacities of the S/C composite were calculated based on the mass of the composite as the cathode-active material. Cyclic voltammetry (CV) measurements were performed on a CHI 600A electrochemical workstation (Shanghai Chenhua, China) with a scan rate of 0.1 mV s^{-1} in the potential range of 1.7–2.8 V (*vs.* Li/Li^+). In addition, electrochemical impedance spectra (EIS) were performed using a Zahner IM6ex electrochemical workstation in the frequency range of 10 mHz to 100 kHz while the disturbance amplitude was set to be 5 mV.

Results and discussion

The schematic diagram of the preparation of the S/A-MCxy composites is shown in **Fig. 1**. Firstly, carbon black is mixed with multi-walled CNTs; then, the mixture goes through a ball-milling process followed by a KOH activation to yield hybrid A-MCxy carbon substrates; finally, sulfur is introduced into A-MCxy to obtain the S/A-MCxy composites. Here, sulfur is mainly trapped in the abundant pores of carbon black, and the web-like structure of CNTs offers highly conductive pathways for both Li ions and electrons. Of course, the extra sulfur exists over the whole surface of the hybrid carbon substrate as the result of large sulfur content in the as-prepared composites.

TG method is proceeded to confirm the sulfur contents in the as-prepared S/A-MCxy composites as indicated in **Fig. 2**. The weight of pure sulfur suffers a sharp decrease at the temperature range from 180 to 320 ℃. However, in the case of the composites, the temperature of the weight loss is retarded 10–30 ℃, which indicates the combination between the carbon substrates and sulfur. The sulfur contents of the S/A-MCxy composites can be obtained directly from the TG curves. (81.7 wt% for the S/A-MC11 composite mainly discussed here) Moreover, the carbon substrates also suffer weight loss from about 90 to 310 ℃, resulted from the dehydration of oxygen-containing functional groups by the activation of KOH (**Fig. S1**). However, the hybrid carbon substrate, taking A-MC11 as the example, does not suffer the weight loss after the same heat treatment as compared with the as-prepared composites. It is the exact reason that the sulfur contents in the as-prepared composites are a little higher than the designed value (80 wt%). In addition, the three carbon substrates have different weight loss. The exact values of weight loss are presented in **Table S1**. The higher the value of the weight loss, the deeper the degree of the activation for porous carbon black.

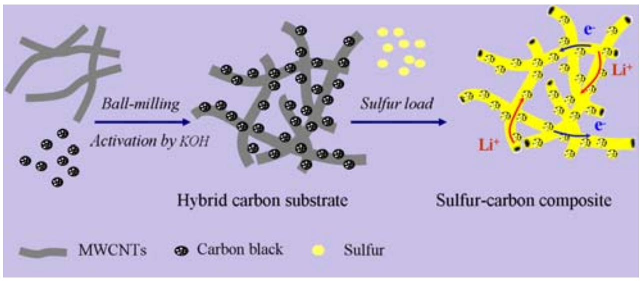

Fig. 1 Schematic illustration of the preparation for the S/A-MCxy composites. Also the transfer of electrons (blue line) and Li ions (red line) in the web-like structure of CNTs is shown in this figure.

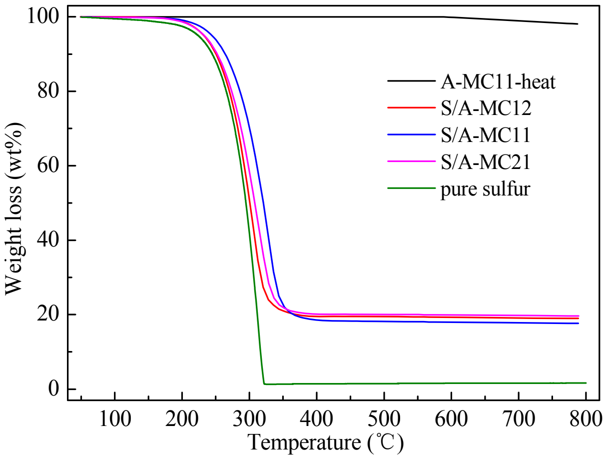

Fig. 2 TG curves of pure sulfur, the S/A-MCxy composites and the A-MC11 carbon substrate, which has the same heat treatment with the as-prepared composites, recorded under an argon atmosphere with the heating rate of 10 ℃ min^{-1}.

XRD patterns of pure sulfur, the as-prepared S/A-MC11 composite and the electrode slices before/after cycling (coated on Al foil) are given in **Fig. 3**. Obviously, with the high sulfur content in the composite, sulfur exists in a crystalline state with sharp diffraction peaks matching well with those of the orthorhombic sulfur (S_8, PDF#08-0247) (**Fig. 3b**). It is believed that sulfur melts and diffuses into the pores of the carbon black matrix leading to an amorphous state while the sulfur content is relatively low. On the contrary, when the sulfur content further increases, the extra sulfur is compelled to aggregate and crystallize on the whole surface of the hybrid carbon substrate, resulting in the sharp peaks of XRD patterns.[22,25] As to the electrode films, the pristine one shows diffraction peaks of crystalline sulfur and those of Al foil at 65.0° and 78.1° (**Fig. 3c**). After 150 discharge/charge cycles, except for the two sharp peaks of Al foil, the electrode film shows a sharp diffraction peak at 31.2°, which can be attributed to that for (044) plane of sulfur. This indicates that crystalline sulfur in the composite can be regenerated after prolonged discharge/charge cycles.

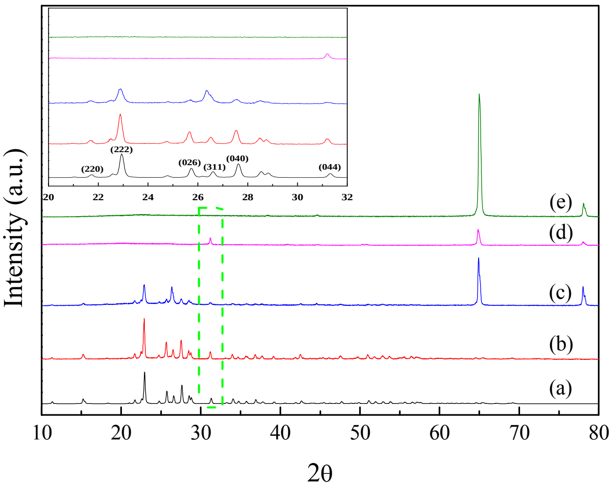

Fig. 3 XRD patterns of a) pure sulfur; b) the S/A-MC11 composite; c) the S/A-MC11 electrode film before discharge; d) the S/A-MC11 electrode film at full charged state after 150 discharge/charge cycles; e) the blank electrode film consisted of Super P and PVDF. The upper-left inset shows a clear observation with 2θ range of 20°–32°. (All tested electrode films were coated on Al foil)

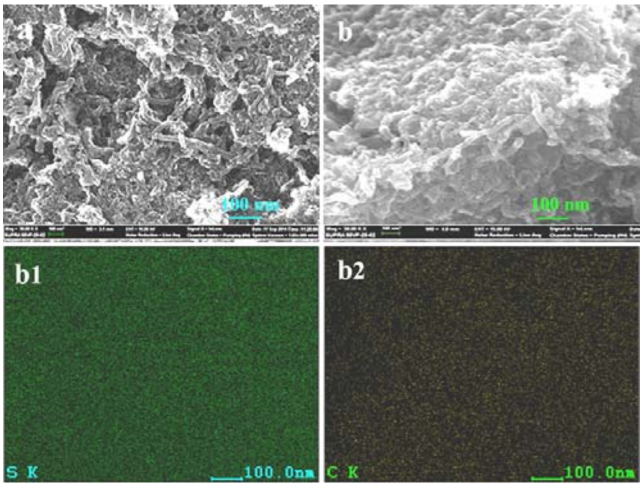

Fig. 4 SEM images of (a) the A-MC11 carbon substrate and (b) the as-prepared S/A-MC11 composite; (b1 and b2) the elemental mapping of the as-prepared S/A-MC11 composite.

SEM images of the A-MC11 hybrid carbon substrate and the as-prepared S/A-MC11 composite are presented in **Fig. 4**. Firstly, the carbon black appears as loose aggregations of carbon spheres with size of 10–20 nm as shown in **Fig. S2**. In the hybrid carbon substrate obtained via ball-milling and the following KOH activation, the individual morphology of the two carbon (carbon black and CNTs) components remains. It is also found that multi-walled CNTs are intertwined with one other to form a conductive network and the carbon black are filled in the gap of the network. This open structure is beneficial for obtaining high sulfur content, promoting the electrolyte infiltration and accommodating the volumetric expansion of S/Li_2S during cycling in the electrochemical reaction. As to the S/A-MC11 composite, there are no apparent differences in morphology, except that the appearance becomes smoother due to the existence of the extra sulfur on the whole surface of the hybrid carbon substrate. Further evidence of sulfur existence in the composite is provided by the elemental mapping of the S/A-MC11 composite as shown in **Fig. 4**b1. Sulfur exists in the S/A-MC11 composite with a uniform distribution.

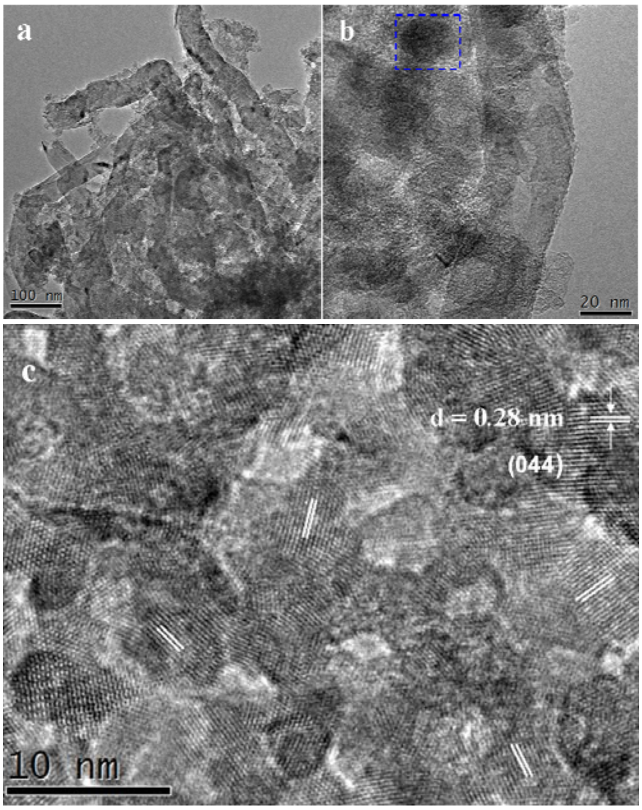

Fig. 5 TEM images of the as-prepared S/A-MC11 composite (a, b and c). Fig. 5c is the high-magnification of the selected area of Fig. 5b as marked by the blue rectangle.

To further illustrate the microstructure of the S/A-MC11 composite, TEM images are provided in **Fig 5**. In the designed structure of the hybrid carbon substrate, multi-walled CNTs are intertwined with one another to form a web-like structure; carbon black is either forced into the inner diameter of multi-walled CNTs, or attached to the outer wall of CNTs as shown in **Fig. S3.** In the case of the S/A-MC11 composite, a more visualized observation of the web-like structure of CNTs is presented in **Fig. 5**a. It is clear that a certain amount of sulfur can diffuse into the pores of carbon black with highly uniform distribution.[22,25] However, when the sulfur content further increases, some small crystalline sulfur nanoparticles appear clearly as dark dots based on the mass-thickness contrast (**Fig. 5**b). With high sulfur content in the composite, the extra sulfur is compelled to aggregate and crystallize on the surface of the substrate, which is in consistent with the XRD patterns as shown in **Fig. 3**. In HRTEM image with a focus on those dark dots, the 0.28 nm lattice fringes with different orientations, corresponding to the (044) plane of sulfur, can be seen clearly in **Fig. 5**c. Actually, the dark dots are polycrystalline sulfur by the aggregation of sulfur nanocrystallites with size of 5–8 nm. With the designed hybrid structure of CNTs and carbon black, the carbon substrate with a web-like conductive structure is obtained for the fast transfer of both electrons and Li ions as shown in **Fig. 1**, which could be beneficial for the electrochemical performance of the as-prepared composites.

Typical cyclic voltammograms (CVs) of the as-prepared S/A-MC11 composite is shown in **Fig. 6**. It is found from CV curves that there are two cathodic peak potentials at 2.27 V and 2.03 V (*vs.* Li/Li^+), which are associated with the two-step reduction of sulfur in the presence of Li ion. In the subsequent anodic scan, only one sharp oxidation peak is observed at 2.39 V which is attributed to the oxidation of insoluble low-order lithium sulfides (Li_2S and Li_2S_2) to soluble high-order lithium sulfides (Li_2S_x, $4 \leq x \leq 8$) and element sulfur. The CV curves of the S/A-MC11 composite show good stability within 5 cycles, implying perfect cycle performance.

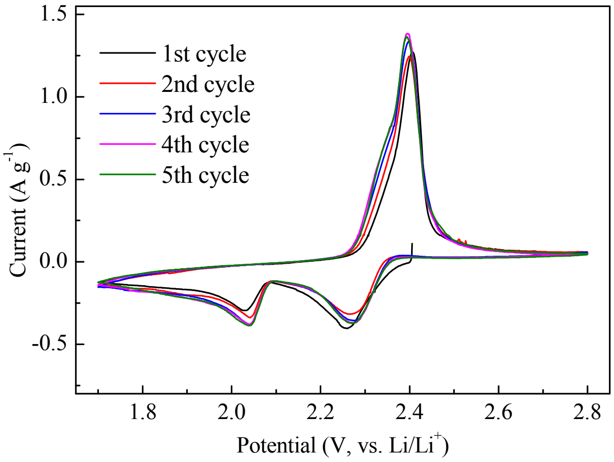

Fig. 6 Cyclic voltammograms of the as-prepared S/A-MC11 composite at the scan rate of 0.1 mV s^{-1}.

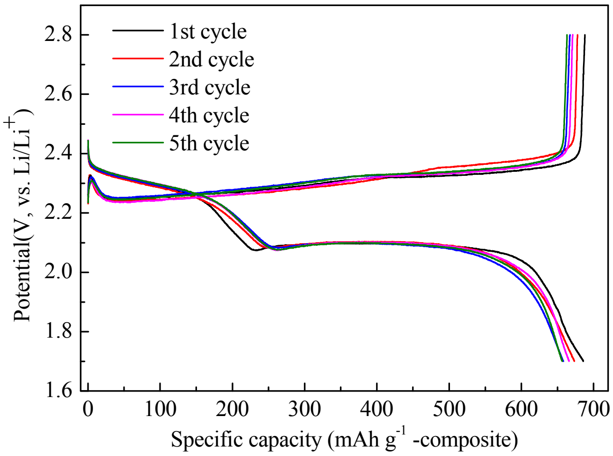

Fig. 7 The initial five charge-discharge curves of the as-prepared S/A-MC11 composite at the current density of 160 mA g^{-1}(composite).

The initial five charge/discharge curves at the current density of 160 mA g^{-1}(composite) are shown in **Fig. 7**. All the discharge curves show two plateaus in the potential profile that are well consistent with the appearance of cathodic peaks in CV curves. The charge/discharge potential plateaus do not drop during cycling, indicating a good potential stability. In the charge processes, the plateau can be attributed to the conversion from insoluble low-order lithium sulfides (Li_2S and Li_2S_2) to soluble high-order lithium sulfides (Li_2S_x, $4 \leq x \leq 8$) and element sulfur. It is notable that the serious overcharge is not observed in the charge curve, implicating the suppressed shuttle effect and high Coulombic efficiency due to the designed hybrid porous structure of the two carbon components in the ether-based electrolyte with $LiNO_3$ as an additive.

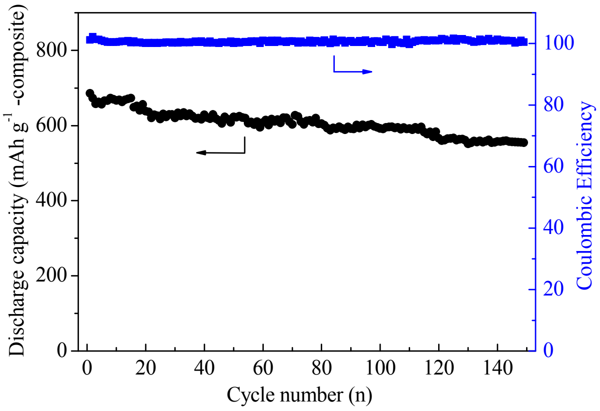

Fig. 8 Cycle performance and the Coulombic efficiency of the S/A-MC11 composite at the current density of 160 mA g^{-1}(composite).

The S/A-MC11 composite exhibits an outstanding cycle performance as given in **Fig. 8**. An initial capacity of 685.9 mA h g^{-1}(composite) is obtained based on the composite as cathode-active material, and the discharge capacity remains at 554.4 mA h g^{-1}(composite) after 150 cycles, indicating a low capacity fading of about 0.12% per cycle. While the mass ratio of CNTs and carbon black changes, the composites exhibit different discharge capacity and cycle stability. As shown in **Fig. S4**, the other two composites (S/A-MC12 and S/A-MC21) deliver lower discharge capacity and poorer cycle stability as compared with the S/A-MC11 composite. The results indicate that an appropriate mass ratio of components in the hybrid carbon substrate is indispensable for achieving excellent electrochemical performance.

The S/A-MC11 composite exhibits good cycle stability owing to the cooperation of CNTs and carbon black in the hybrid substrate. Furthermore, SEM images of the electrode films before/after prolonged cycles are provided in **Fig. 9**. The pristine electrode film presents a loose and porous structure with plentiful interspaces, which is helpful to the penetration of electrolyte in the cathode. After 150 discharge/charge cycles, the deposition and aggregation of insoluble reduction products can be observed with a certain degree. Importantly, the loose and porous structure of the electrode film is still maintained. It means that the satisfying structure can be kept well during long cycling, which is beneficial to the excellent cycle performance of the S/A-MC11 composite.

In addition, the coulombic efficiency reaches about 100% for the composite during cycling. During the initial 20-30 cycles, the $LiNO_3$ additive in the electrolyte has a great impact on decreasing the polysulfide shuttle of the sulfur cathode. With more cycles, $LiNO_3$ additive could be used up on the lithium anode with high reducibility. Meanwhile, the irreversible capacity is also originated from the loss of active material after the large volume change of the sulfur cathode. At this point, the porous structure of the sulfur cathode comes into play an irreplaceable role. Owing to the designed carbon substrate, the cathode presents porous structure both before and after cycling (**Fig. 9**), which is highly important to accommodate the volume expansion and insure the penetration of the electrolyte, resulting in high coulombic efficiency over subsequent cycles.

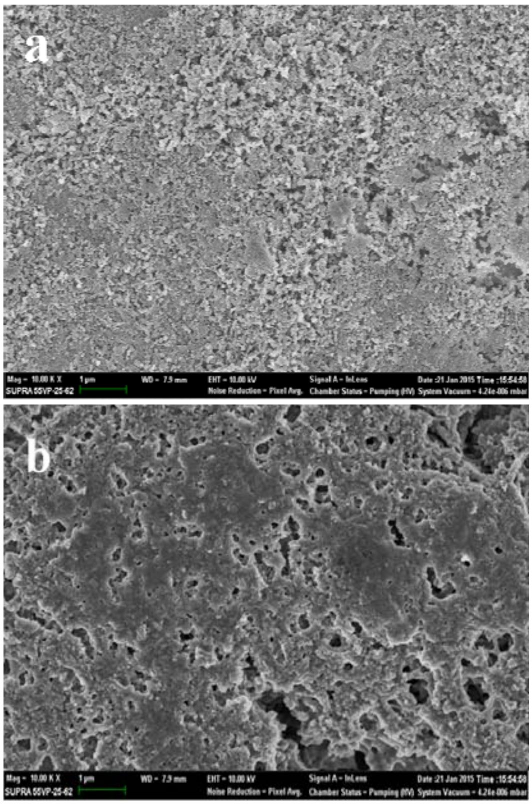

Fig. 9 SEM images of the S/A-MC11 electrode films: a) before cycling; b) after 150 discharge/charge cycles.

Besides, sulfur-based cathodes need to have high sulfur loading to achieve a high practical energy density, thus the S/A-MC11 electrode with higher sulfur loading of 3.0 mg cm^{-2} is also fabricated to make an attempt. The composite exhibits the initial discharge capacity 588.8 mA h g^{-1}(composite) at the current density of 80 mA g^{-1}(composite) and good cycle stability up to 150 cycles at the current density of 160 mA g^{-1}(composite) **(Fig. S5)**. It means that the designed hybrid structure of carbon substrate is beneficial for good performance of the electrode material with high sulfur loading.

The high-rate discharge performance of the as-prepared S/A-MC11 composite is investigated at the current densities of 80, 160, 400, 800, 1600 and 3200 mA g^{-1}(composite), as shown in **Fig. 10**. The composite delivers an initial discharge capacity of 837.3 and 685.9 mA h g^{-1}(composite) at the current densities of 80 and 160 mA g^{-1}(composite). When the current densities are increased to 800, 1600 and 3200 mA g^{-1}(composite), the discharge capacities of 334.9, 278.2 and 234.4 mA h g^{-1}(composite) are obtained for the S/A-MC11 composite, respectively. In comparison with the composite with low sulfur content (43.7 wt % S),[45] the high-rate performance of the S/A-MC11 composite is slightly low. In addition, both the high and low potential plateaus are simultaneously shrunken with increasing the current densities,[57] accompanied with the increase of the discharge capacity (**Fig.6S**). In particular, the shrinkage of the second low potential plateau is more serious. It means that the good dispersion of sulfur nanocrystallites on conductive carbon substrate is highly important for avoiding the irreversible serious deposition and aggregation of insoluble reduction products.

The maximum capacity for composite is 837.3 mA h g^{-1} at the current densities of 80 mA g^{-1}(composite). It means that the sulfur utilization is 61.2%, which is slightly lower as compared to the composite with the low sulfur content.[45] It is noted that the sulfur utilization is highly related to the distribution and existential state of sulfur in the composite. When the sulfur content is low, the sulfur distribution is more homogeneous on the carbon substrate, and almost no crystalline sulfur nanoparticles can be observed in the composite. For the composite with the large sulfur content, some small crystalline sulfur nanoparticles appear (**Fig.5**). As a consequence, those insulating sulfur nanoparticles may reduce the electrical conductivity of the electrode and limit the extent of reaction of sulfur in the electrochemical reaction.

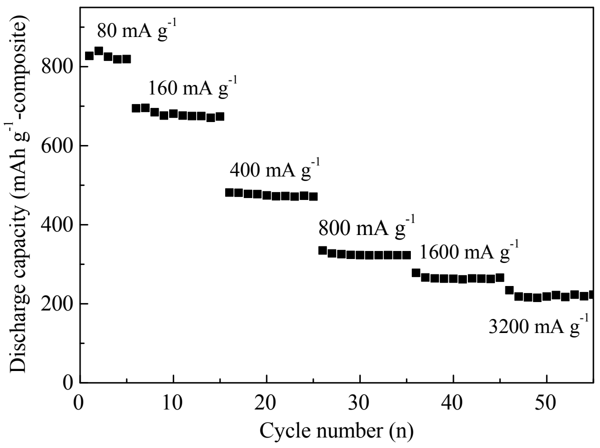

Fig. 10 Rate capability of the as-prepared S/A-MC11 composite at different current densities.

Given the fact that the cycle stability of the composite are mainly associated with the interfacial charge-transfer process and Li ion diffusion process in the composite, electrochemical impedance spectra (EIS) at the fully charged states in different cycles are measured to get a further insight into the reaction mechanism of the S/A-MC11 composite, as presented in **Fig. 11**. It can be found that the impedance plots for all of the fully charged states are consisted of a depressed semicircle in the high-frequency domain and a sloping line in the low-frequency region, which correspond to the charge-transfer process and the semi-infinite Warburg diffusion process, respectively. It is shown from the simulated data using equivalent circuit (**Table S2**) that both the charge-transfer resistance and the semi-infinite Warburg diffusion impedance increase simultaneously. The charge-transfer resistance decreases sharply to the lowest value of 26.4 Ω in the first cycle from 78.2 Ω before discharge, implying the activation of the surface electrochemical activity by the charge/discharge process. In subsequent cycles, the charge-transfer resistance increases gradually to 66.3 Ω in the 100th cycle. With respect to the diffusion process, the Warburg diffusion impedance increases correspondingly from 35.63 Ω in the first cycle to 191.7Ω in the 100th cycle. However, both the charge-transfer resistance and the Warburg diffusion impedance in the 100th cycles are still low than that before discharge for the composite. It indicates that the irreversible deposition and aggregation of insoluble reduction products on the surface of the cathode could be increased gradually during cycling, which is in accordance with the SEM observation of the electrode film (**Fig. 9b**). Of course, those insoluble products could be partially oxidized to element sulfur for the fully charged state (**Fig. 3**), resulting in the increase of both the charge-transfer resistance and Warburg diffusion impedance. Therefore, it is demonstrated that the surface electrochemical activity and the Li ion diffusion capability are gradually decreased during long cycling, leading to the slow capacity decay of the S/A-MC11 composite.

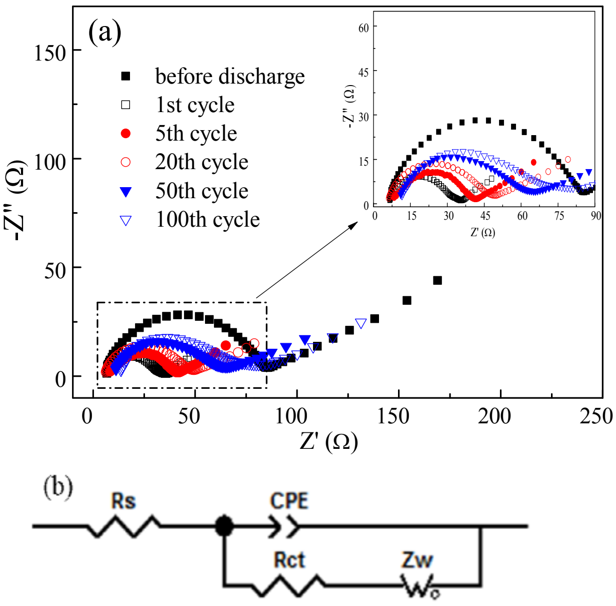

Fig. 11 (a) EIS spectra of the as-prepared S/A-MC11 composite after charged to 2.8 V at the current density of 160 mA g^{-1}(composite); (b) Equivalent circuit was used to fit the experimental data. Rs: the solution resistance; Rct: the charge-transfer resistance; CPE: the constant phase element; Zw: the semi-infinite Warburg diffusion impedance.

The electrochemical performance of the S/C composites is affected by many factors. In the sulfur/carbon black/CNTs composite with high sulfur content, both the web-like structure of CNTs and the abundant pores of carbon black contribute to the improvement of the electrochemical performance of the sulfur cathodes, especially the cycle stability. Of course, a further exploration and development of the multi-composite with sulfur and hybrid carbon substrates would be helpful to obtain sulfur cathodes with the desirable electrochemical performance.

Conclusion

In summary, hybrid carbon substrate, incorporating of the commercial carbon black and multi-walled CNTs, is obtained within simple steps to fix sulfur as cathode for Li-S batteries. The designed hybrid structure contributes to the excellent cycle performance of the S/A-MC11 composites, even though the sulfur content reaches up to 81.7 wt%. In the hybrid substrate, the conductive web-like structure of CNTs benefits the excellent transfer of both Li ions and electrons. Meanwhile, a reasonable mass ratio of the components in the hybrid substrate is really essential for good electrochemical performance. As in this case, the as-prepared S/A-MC11 composite exhibits a low capacity fading about 0.12 % per cycle within 150 cycles, and high Coulombic efficiency of almost 100 % even in the initial cycle at the current density of 160 mA g^{-1}(composite) based on the composite as cathode-active material. This attempt might put forward a low-cost and effortless approach to prepare S/C composites with high electrochemical performance for Li-S batteries.

Acknowledgment

Financial Supports from the 973 Program (2015CB251100), NFSC (21421001), and MOE Innovation Team (IRT13022) of China are gratefully acknowledged.

Notes and references

Institute of New Energy Material Chemistry, Collaborative Innovation Center of Chemical Science and Engineering (Tianjin), Tianjin Key Laboratory of Metal and Molecule Based Material Chemistry, Nankai University, Tianjin 300071, China. E-mail: xpgao@nankai.edu.cn; Fax: +86-22-2350-0876; Tel: +86-22-23500876

1 M. Armand and J. M. Tarascon, *Nature*, 2008, **451**, 652–657.
2 B. Scrosati and J. Garche, *J. Power Sources,* 2010, **195**, 2419–2430.
3 X. L. Ji, K. T. Lee and L. F. Nazar, *Nat. Mater.*, 2009. **8**. 500.
4 X. P. Gao and H. X. Yang, *Energy Environ. Sci*., 2010, **3**, 174.
5 P. G. Bruce, S. A. Freunberger, L. J. Hardwick and J. M. Tarascon, *Nat. Mater.,* 2012, **11**, 19.
6 X. L. Ji and L. F. Nazar, *J. Mater. Chem.*, 2010, **20**, 9821–9826.
7 D. Marmorstein, T. H. Yu, K. A. Striebel, F. R. McLarnon, J. Hou and E. J. Cairns, *J. Power Sources,* 2000, **89**, 219.
8 J. Shim, K. A. Striebel and E. J. Cairns, *J. Electrochem. Soc*., 2002, **149**, A1321–A1325.
9 H. S. Ryu, H. J. Ahn, K. W. Kim, J. H. Ahn and J. Y. Lee, *J. Power Sources,* 2006, **153**, 360–364.
10 A. Manthiram, Y. Fu and Y. S. Su, *Acc. Chem. Res.*, 2013, **46**, 1125.
11 S. S. Zhang, *J. Power Sources*, 2013, **231**, 153–162.
12 J. Gao and H. D. Abruna, *J. Phys. Chem. Lett*., 2014, **5**, 882–885.
13 G. L. Xu, Q. Wang, J. C. Fang, Y. F. Xu, J. T. Li, L. Huang and S. G. Sun, *J. Mater. Chem. A*, 2014, **2**, 19941.
14 J. M. Zheng, M. Gu, H. H. Chen, P. Meduri, M. H. Engelhard, J. G. Zhang, J. Liu and J. Xiao, *J. Mater. Chem. A*, 2013, **1**, 8464.
15 D. J. Lee, M. Agostini, J. W. Park, Y. K. Sun, J. Hassoun and B. Scrosati, *ChemSusChem,* 2013, **6**, 2245–2248.
16 R. Xu, I. Belharouak, J. C. M. Li, X. F. Zhang, I. Bloom and J. Bareo, *Adv. Energy Mater.*, 2013, **3**, 833–838.
17 K. Jeddi, M. Ghaznavi and P. Chen, *J. Mater. Chem. A*, 2013, **1**, 2769-2772.
18 E. S. Shin, K. Kim, S. H. Ohand and W. I. Cho, *Chem. Commun.*, 2013, **49**, 2004.
19 J. J. Hu, G. K. Long, S. Liu, G. R. Li and X. P. Gao, *Chem. Commun.*, 2014, **50**, 14647.
20 W. G. Wang, X. Wang, L. Y. Tian, Y. L. Wang and S. H. Ye, *J. Mater. Chem. A,* 2014, **2**, 4316–4323.
21 Y. Z. Zhang, S. Liu, G. C. Li, G. R. Li and X. P. Gao, *J. Mater. Chem. A*, 2014, **2**, 4652–4659.
22 C. Lai, X. P. Gao, B. Zhang, T. Y. Yan and Z. Zhou, *J. Phys. Chem. C,* 2009, **113**, 4712.
23 S. R. Chen, Y. P. Zhai, G. L. Xu, Y. X. Jiang, D. Y. Zhao, J. T. Li, L. Huang and S. G. Sun, *Electrochim. Acta*, 2011, **56**, 9549–9555.
24 W. H. Zhang, D. Qiao, J. X. Pan, Y. L. Cao. H. X. Yang and X. P. Ai, *Electrochim. Acta*, 2013, **87**, 497–502.
25 B. Zhang, X. Qin, G. R. Li and X. P. Gao, *Energy Environ. Sci*., 2010, **3**, 1531–1537.
26 X. L. Li, Y. L. Cao, W. Qi, L. V. Saraf, J. X, Z. M. Nie, J. Mietek, J. G. Zhang, B. Schwenzer and J. Liu, *J. Mater. Chem.,* 2011, **21**, 16603.
27 G. C. Li, J. J. Hu, G. R. Li, S. H. Ye and X. P. Gao, *J. Power Sources*, 2013, **240**, 598–605.
28 N. Jayaprakash, J. Shen, S. S. Moganty, A. Corona and L. A. Archer, *Angew. Chem. Int. Ed.*, 2011, **50,** 5904–5908.
29 C. F. Zhang, H. B. Wu, C. Z. Yuan, Z. P. Guo and X. W. Lou, *Angew. Chem. Int. Ed*., 2012, **51,** 9592–9595.
30 S. Q. Chen, X. D. Huang, B. Sun, J. Q. Zhang, H. Liu and G. X. Wang, *J. Mater. Chem. A*, 2014, **2** 16199.
31 H. Xu, Y. F. Deng, Z. C. Shi, Y. X. Qian, Y. Z. Meng and G. H. Chen, *J. Mater. Chem. A*, 2013, **1**, 15142.
32 B. Ding, C. Z. Yuan, L. F. Shen, G. Y. Xu, P. Nie, Q. X. Lai and X. G. Zhang, *J. Mater. Chem. A*, 2013, **1**, 1096–1101.
33 Y. S. Su, Y. Z. Fu and A. Manthiram, *Phys. Chem. Chem. Phys.*, 2012, **14**, 14495–14499.
34 J. J. Chen, Q. Zhang, Y. N. Shi, L. L. Qin, Y. Cao, M. S. Zheng and Q. F. Dong, *Phys. Chem. Chem. Phys.,* 2012, **14**, 5376–5382.
35 W. Ahn, K. B. Kim, K. N. Jung, K. H. Shin and C. S. Jin, *J. Power Sources,* 2012, **202**, 394–399.
36 J. Q. Huang, Q. Zhang, S. M. Zhang, X. F. Liu, W. C. Zhu, W. Z. Qian and F. Wei, *Carbon*, 2013, **58**, 99–106.
37 F. Wu, J. Z. Chen, L. Li, T. Zhao, Z. Liu and R. J. Chen, ChemSusChem., 2013, 6, 1438–1444.
38 L. Sun, M. Y. Li, Y. Jiang, W. B. Kong, K. L. Jiang, J. P. Wang and S. S. Fan, *Nano Lett.,* 2014, **14**, 4044–4049.
39 Z. B. Xiao, Z. Yang, H. G. Nie, Y. Q. Lu, K. Q. Yang and S. M. Huang, *J. Mater. Chem. A*, 2014, **2**, 8683.
40 Z. Yuan, H. J. Peng, J. Q. Huang, X. Y. Liu, D. W. Wang, X. B. Cheng and Q. Zhang, *Adv. Funct. Mater.*, 2014, **24**, 6105–6112.
41 X. Pu, G. Yang and C. Yu, *Adv, Mater.*, 2014, **26**, 7456–7461.
42 M. M. Rao, X. Y. Song, H. G. Liao and E. J. Cairns, *Electrochim. Acta,* 2012, **65**, 228.
43 L. C. Yin, J. L. Wang, J. Yang and Y. N. Nuli, *J. Mater. Chem*., 2011, **21**, 6807.
44 F. Wu, J. Z. Chen, R. J. Chen, S. X. Wu, L. Li, S. Chen and T. Zhao, *J. Phys. Chem. C*, 2011, **115**, 6057.
45 G. C. Li, G. R. Li, S. H. Ye and X. P. Gao, *Adv. Energy Mater*., 2012, **2**, 1238.
46 L. C. Yin, J. L. Wang, F. J. Lin, J. Yang and Y N. Nuli, *Energy Environ. Sci*., 2012, **5**, 6966–6972.
47 W. Y. Li, Q. F. Zhang, G. Y. Zheng, Z. W. Seh, H. B. Yao and Y. Cui, *Nano Lett.*, 2013, **13,** 5534–5540.
48 C. Wang, W. Wan, J. T. Chen, H. H. Zhou, X. X. Zhang, L. X. Yuan and Y. H. Huang, *J. Mater. Chem. A,* 2013, **1**, 1716.
49 D. L. Wang, Y. C. Yu, W. D. Zhou, H. Chen, F. J. Disalvo, D. A. Mullercd and H. D. Abruna, *Phys. Chem. Chem. Phys*., 2013, **15**, 9051–9057.
50 S. Xin, L. Gu, N. H. Zhao, Y. X. Yin, L. J. Zhou, Y. G. Guo and L. J. Wan, *J. Am. Chem. Soc.,* 2012, **134**, 18510–18513.
51 R. J. Chen, T. Zhao, J. Lu, F. Wu, L. Li, J. Z. Chen, G. Q. Tan, Y. S. Ye and K. Amine, *Nano Lett.,* 2013, **13**, 4642–4649.
52 S. T. Lu, Y. W. Cheng, X. H. Wu and J. Liu, *Nano Lett.,* 2013, **13**, 2485–2489.
53 J. Xie, J. Yang, X. Y. Zhou, Y. L. Zou, J. J. Tang, S. C. Wang and F. Chen, *J. Power Sources,* 2014, **253**, 55–63.
54 X. Yang, L. Zhang, F. Zhang, Y. Huang and Y. S. Chen, *ACS Nano,* 2014, **8**, 5208–5215.
55 B. Wang, Y. F. Wen, D. L. Ye, H. Yu, B. Sun, G. X. Wang, D. H. Jurcakova and L. Z. Wang, *Chem. Eur. J*., 2014, **20**, 1–8.
56 Y. M. Chen, X. Y. Li, K. S. Park, J. H. Hong, J. Song, L. M. Zhou, Y. W. Mai, H. T. Huang and J. B. Goodenough, *J. Mater. Chem. A*, 2014, **2**, 10126.
57 M. Ghaznavi and P. Chen, *J. Power Sources,* 2014, **257**, 402–411.